China Instrument and Control Society
Instrumentation
OPEN ACCESS
INSTRUMENTATION, Vol. 13, No. 2, June 2026 https://doi.org/10.15878/j.instr.202600309

Article

PELT-Phase LSTM Method for Mach Number Prediction of Wind Tunnel Flow Field

Luping Zhao*, Tingting Li

College of Information Science and Engineering, Northeastern University, Shenyang 110819, Liaoning Province, China

* Corresponding author email: zhaolp@ise.neu.edu.cn

Abstract: The stability of the Mach number plays a key role in wind tunnel flow field performance. To facilitate the direct processing of continuous 3D transonic wind-tunnel data and improve the accuracy of Mach number prediction, this paper proposes a new method based on the Pruned Exact Linear Time-Phase Long Short-Term Memory model. First, the PELT variable-point detection algorithm is employed to partition the data into intervals. Subsequently, based on the characteristics of the linearized models for each interval, K-means clustering is applied to segment the data into three phases: the start stage, the steady stage, and the transition stage. Finally, LSTM models are applied for prediction in each phase, with comparative experiments conducted against a global LSTM model, a global Multi-Layer Perceptron (MLP) model, and a global Radial Basis Function (RBF) model. Results demonstrate that, compared to other models, the proposed approach reduces the root mean square error (RMSE) by an average of 36.74% at Mach 0.3 and 51.19% at Mach 0.8, indicating very high prediction accuracy and good stability.

Keywords: continuous wind tunnel; three-dimensional processing; mach number prediction; PELT-Phase LSTM model

Citation: Luping Zhao, Tingting Li."PELT-Phase LSTM Method for Mach Number Prediction of Wind Tunnel Flow Field." Instrumentation 13, no.2 (June 2026). https://doi.org/10.15878/j.instr.202600309

1 Introduction

In recent years, the rapid development of flight technology and the continuous emergence of various new types of aerospace vehicles have imposed higher technical demands and control accuracy requirements on wind tunnel testing. As an important platform for aerodynamic performance verification and parameter evaluation in the aerospace field, wind tunnels play an irreplaceable role in vehicle development, parameter evaluation, and engineering verification[1]. In the process of wind tunnel testing, Mach number is an important parameter to characterize the airflow velocity, and its stability directly affects the characteristics of the flow field, the reliability of the test results, and the validity of the model data. Therefore, improving the control and prediction accuracy of Mach number has been the research focus of academia and engineering design.

Studies have been conducted to establish Mach number prediction models mainly based on physical information or data-driven methods, such as Ren et al.[2], who fused the RANS equations with data-driven turbulent viscosity modeling to achieve the global flow field prediction in the viscous/non-viscous region within the Mach number interval of 0.3-0.7. Zhao et al. [3] constructed an NARX-Elman prediction framework and designed an IOSBC-GA migration strategy, which optimizes historical model parameters using limited new operating condition data. The prediction accuracy of this method is significantly better than that of the traditional model, and the error of the migrated model is 73% lower than that of the non-migrated model. Gao et al. [4] proposed a feedforward control based on Gaussian process regression combined with a PID control strategy to improve the Mach number control accuracy in continuous sweep mode.

Despite these advancements in Mach number control and prediction, considering that the Mach number in wind tunnel experiments shows a significant phase pattern, such global modeling approaches struggle to adequately capture the phase-specific dynamics of the Mach number during wind tunnel operation, and only limited studies have addressed the characteristics of the Mach number changes at different phases. For example, Wang[5] proposed a two-phase hybrid model for Mach number prediction, which utilizes the recursive Pseudo-NARX to predict the Mach number in the dynamic stamping phase, and the NARX to predict the steady state stabilization phase, which significantly improves the prediction accuracy and reduces the prediction error.

In addition, wind tunnel experimental data belong to the typical three-dimensional (3D) structure characterized by tightly coupled temporal, parametric, and batch dimensions. However, traditional preprocessing methods mostly unfold 3D data into 2D slices and then model the 2D data. For example, Ju et al. [6] established multiple local models by dividing the working conditions, switched the optimal model with the output error integral index, and used a dynamic matrix control algorithm to realize the fast response. This method achieves disturbance-free transition during condition switching, and the Mach number control accuracy reaches 0.00056. Sun et al. [7] divide the incoming stream into three conditions according to the Mach number in the low-speed domain, subsonic, and transonic, and expand the lobe load distribution into the chordwise position-Mach-number function within the transonic region to optimize the surge position control. This two-dimensional treatment tends to ignore the time-dependent and batch-to-batch evolution laws, limiting the predictive ability and generalization performance of the model.

In recent years, some scholars have also attempted to use a convolutional neural network (CNN) for 3D spatial modeling of wind tunnel data, e.g., by normalizing and reconstructing the wind tunnel 3D data into image form and extracting spatial features, which preserves the integrity of the original data to a certain extent and improves the prediction accuracy [8].

Based on the above problems, this paper proposes a Mach number prediction method that integrates change-point detection and phase long short-term memory network (LSTM) modeling for the phase characteristics presented by Mach number and the three-dimensional characteristics of wind tunnel test data. This method first employs the PELT algorithm to perform interval-adaptive segmentation on the wind tunnel Mach number sequence. Based on the linear characteristics of each interval, the K-means clustering algorithm is used to divide the sequence into three phases: start stage, steady stage, and transition stage[9-11], with each phase comprising multiple sub-intervals. Subsequently, an LSTM model is constructed for each phase to predict the Mach number. Finally, the prediction results from the staged models are compared and analyzed against those from traditional global LSTM models, global RBF models, and global MLP models. This method not only better captures the batch and time series features in the sequence but also significantly improves the accuracy and stability of the Mach number prediction, which provides a new idea for high-precision Mach number control in wind tunnel testing.

2 PELT-Phase LSTM Model

2.1 PELT Algorithm

To learn the feature similarity across different phases of the data, it is necessary to first divide the input data into intervals for subsequent batch processing. In this paper, variable point detection is implemented using the PELT algorithm (Pruned Exact Linear Time), which is a change point detection algorithm based on dynamic programming and pruning techniques[12], aiming at identifying the time points in a time series where the statistical characteristics change significantly based on the features such as mean and variance.

The algorithm aims to minimize the overall penalty function to determine the location of the change point in the global optimum, which is mathematically formulated as follows: assuming a given time series $\{y_1, y_2, y_3, \cdots, y_n\}$, it is desired to determine a set of change points $\{\tau_1, \tau_2, \cdots, \tau_m\}$ to divide the sequence into m+1 intervals, minimizing the following objective function:

$$C\left(y_{1:n}\right) = \sum_{i=1}^{m+1}\left(cost\left(y_{\tau_{i-1}+1:\tau_i}\right)\right) + \beta m \tag{1}$$

Where, $y_{1:n}$ is the time series data; $cost(y_{\tau_{i-1}+1:\tau_i})$ denotes the penalty between the intervals from the change point $(\tau_{i-1}+1)$ to τ_i; m is the number of change points; and β is the regularization penalty term, which is used to control the change point data to prevent overfitting.

The core of the PELT algorithm lies in constructing dynamic planning transfer equations to recursively calculate the minimum total penalty at each time node. To improve the computational efficiency, PELT is based on the principles of "optimal substructure" and "subadditivity of penalty function", and utilizes the pruning strategy during the dynamic planning process to timely eliminate the candidate variables that are unlikely to produce an optimal solution. The steps of the algorithm are as follows:

(1)Initialization: Set the initial state and record the optimal cost from the start time point to the first change point.

(2)Recursion: use dynamic programming to calculate the optimal cost of each time point, and eliminate certain unnecessary candidate solutions according to the pruning condition during the calculation process.

(3)Update change points: record possible change point positions at each iteration.

(4)Terminate: after completing the computation of

all time points, output the found optimal sequence of variation points.

At present, the PELT algorithm is widely used for processing time series data with obvious phase changes. For example, Li et al.[13] applied the PELT algorithm to achieve the detection of time series mutation points, accurately identified the statistical characteristics of freight turnover jumps through dynamic planning optimization and penalty term control, and constructed a fusion framework by combining grey correction and SARIMA modeling, which significantly improved the prediction accuracy of highly volatile data. Chen et al. [14] combined PELT with the ADF test to achieve fine identification of traffic states through adaptive segmentation of standardized sequences, and finally reached a short-term prediction interval with more than 80% coverage. Considering the typical phase characteristics presented by the Mach number change process, the PELT algorithm is used in this paper for the adaptive phase segmentation of the wind tunnel Mach number sequence to assist the subsequent phased modeling and prediction.

2.2 LSTM Model

Long Short-Term Memory (LSTM) was proposed by Hochreiter and Schmidhuber in 1997[15], which was designed to solve the gradient vanishing and gradient explosion problems encountered by Recurrent Neural Networks (RNN) when learning long-term dependencies. The core idea of the model lies in the introduction of memory units and three gating mechanisms (input gate, forgetting gate, and output gate) to effectively learn and retain long-term dependency information through selective memorization and forgetting, and its schematic diagram is shown below.

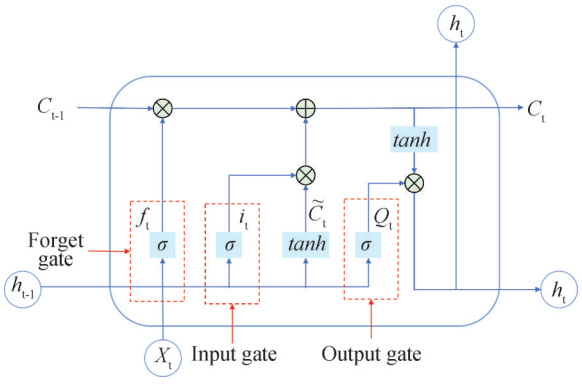

Fig.1 LSTM schematic diagram

The forgetting gate determines which information in the cell state to forget, based on the current input and the previous hidden state. Passing these two through a fully connected layer and applying a sigmoid function maps the output to [0,1], where 0 means completely forgotten, and 1 means completely retained. The corresponding formula is as follows:

$$f_t=\sigma\left(W_f\cdot\left[h_{t-1},x_t\right]+b_f\right) \tag{2}$$

Where W_f is the weight matrix, b_f is the bias term, h_{t-1} is the hidden state at the previous moment, x_t is the input at the current moment, and σ denotes the sigmoid function.

The input gate determines what new information needs to be written to the cell state. This consists of two parts: one part is the input gate, which decides which parts of the memory cell we will update; the other part is a tanh layer, which creates a new vector of candidate values that may be added to the memory cell. The corresponding formula is as follows:

Input gate value:

$$i_t=\sigma\left(W_i\cdot\left[h_{t-1},x_t\right]+b_i\right) \tag{3}$$

Candidate values:

$$\tilde{C}_t=\tanh\left(W_C\cdot\left[h_{t-1},x_t\right]+b_C\right) \tag{4}$$

Where, W_i, W_C are weight matrices, b_i, b_C are bias terms, h_{t-1} is the hidden state of the previous moment, x_t is the input of the current moment, σ is the sigmoid function, and tanh is the hyperbolic tangent function.

According to the update mechanism of the forgetting gate and input gate, the update of the memory cell can be carried out. The updated cell state formula is as follows:

$$C_t=f_t\cdot C_{t-1}+i_t\cdot\tilde{C}_t \tag{5}$$

where f_t is the output of the oblivion gate, C_{t-1} is the cell state at the previous moment, i_t is the input gate value, and $\tilde{C}_t$ is the candidate value.

The output gate determines the output of the current moment and which information will flow from the cell state to the hidden state. Based on the input of the current moment and the hidden state of the previous moment, the value of the output gate is normalized to the interval [0,1] through a fully connected layer and applying a sigmoid function, where 0 means no output at all and 1 means full output. The cell state is then passed through the tanh layer, and the result is normalized to the interval [-1, 1] and multiplied by the value of the output gate to obtain the final hidden state. The corresponding formula is as follows:

$$o_t=\sigma\left(W_o\cdot\left[h_{t-1},x_t\right]+b_o\right) \tag{6}$$

$$h_t=o_t\cdot\tanh\left(C_t\right) \tag{7}$$

Where, W_o is the weight matrix, b_o is the bias term, h_{t-1} is the hidden state at the previous moment, x_t is the current input, σ is the sigmoid function, C_t is the current cell state, and tanh is the hyperbolic tangent function.

Since LSTM models can capture long-time dependencies and have no gradient vanishing problem, they have been widely used by scholars for the prediction of fluid parameters. For example, Du et al.[16] constructed a multilayer LSTM network to achieve high-precision wind pressure time-range prediction for 44 measurement points on the surface of a square column by embedding the spatial coordinates of the measurement points and the time-range input of the wind pressure at the center position. Junjie Zhang et al.[17] utilized an LSTM network to process the pseudo time series data formed by the

change of angle of attack, and captured the nonlinear dependence of aerodynamic parameters evolving dynamically with the angle of attack through its gating mechanism, which effectively improved the prediction accuracy of the variable confidence fusion model. Therefore, in order to fully learn the time series dependence law of wind tunnel test data, this paper constructs an LSTM model for Mach number prediction.

2.3 Overall Algorithm Flow

Combining the methods mentioned in 2.1 and 2.2 above, to fully learn the timing dependence of wind tunnel 3D data and the evolution law between batches, and to improve the accuracy of Mach number prediction, this paper establishes a PELT-phase LSTM model, which divides the intervals by the PELT change-point detection algorithm, and divides them into three phases according to the characteristic parameters of the intervals: the start stage, the steady stage, and the transition stage, and employs phase-specific LSTMs to predict the data of each phase separately. All models were executed in Python 3.12 on Windows 10 with 16.0 GB DDR4 RAM, an AMD Ryzen 5 5600H 3.3 GHz processor, and an NVIDIA GeForce RTX 3060 Laptop GPU. The overall flow of the algorithm is shown in Fig.2.

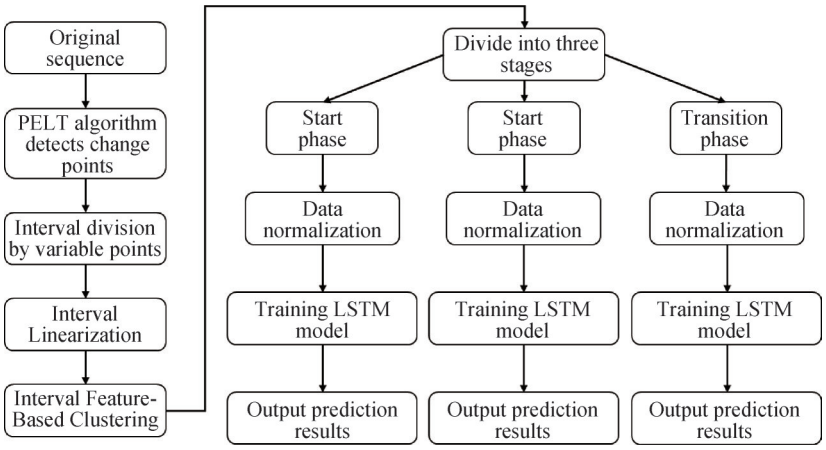

Fig. 2 Flow chart of the overall algorithm

3 Description of Wind Tunnel System

3.1 Wind Tunnel System Structure

The object of this paper is a 0.6 m room-temperature transonic continuous closed-circuit wind tunnel, and it is necessary to fully understand and analyze its structure before conducting subsequent Mach number numerical experiments.

The layout of the continuous transonic wind tunnel is shown in Fig.3, which mainly consists of a stabilization section, a test section, an adaptive second throat, a return circuit, a high-speed diffusion section, a compressor, a low-speed diffusion section, a heat exchanger, and a corner section, etc., and the functions of each component are as follows: the main compressor is responsible for driving the main circuit airflow and controlling the Mach

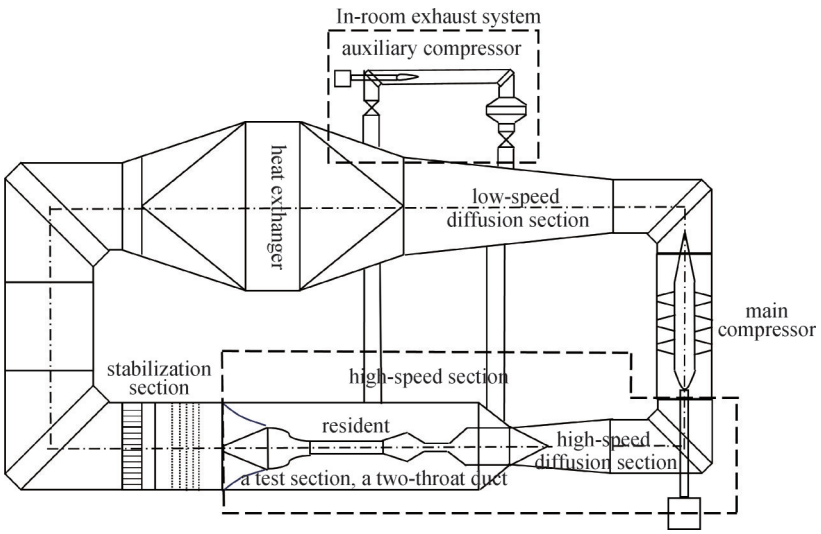

Fig.3 Overall structure of the continuous wind tunnel

number of the test section through speed regulation, and the auxiliary compressor regulates pumping capacity to optimize the main compressor's operating point, enhancing total pressure recovery in the diffuser [18]. The two are connected by piping to form a closed airflow circuit. The boundary layer suction system extracts the airflow from the surface layer of the test section and returns it to the main circuit after the second throat, which is combined with the adjustment of the second throat to realize the precise control of the Mach number. The control system adopts a constant Mach number operation mode, through the closed-loop adjustment of the main compressor speed to maintain the target Mach number, and the auxiliary compressor speed is adjusted sequentially to obtain the matching characteristics of different pumping capacities, to ensure the synergy of the main and auxiliary compressors and the stable operation of the wind tunnel.

To ensure stable operation of the wind tunnel, the auxiliary system controls the total temperature and pressure of the stabilized section to remain constant, and the Mach number is controlled by adjusting the main compressor speed, supplemented by the two-throat channel and the standing room pumping system.

3.2 Experimental Evaluation Index

For the wind tunnel flow field control system, the model fidelity directly affects the stability and accuracy of the subsequent control Mach number. In order to better evaluate the proposed model and facilitate the comparison and analysis of the experimental results, this paper chooses the root mean square error (RMSE) to quantify prediction accuracy.

RMSE is a common indicator of the difference between predicted and actual values, which indicates the square root of the average squared deviations between predicted and actual values. The smaller the value of RMSE, the closer the predicted value is to the true value, and the better the prediction of the model is.

$$RMSE = \sqrt{\frac{1}{K}\sum_{k=1}^{K}\left(M_p(k) - M_r(k)\right)^2} \tag{8}$$

Where, $M_p(k)$ is the predicted value of the Mach number, $M_r(k)$ is the real value of the Mach number, and K is the number of sampling points.

4 Results and Discussion

In this paper, the modeling and Mach number prediction are carried out on the data from the 0.6 m wind tunnel with sufficient experimental data. Mach 0.3 represents stable flow conditions with mild nonlinear characteristics, typical of basic subsonic operations. Mach 0.8 corresponds to transonic critical conditions approaching the speed of sound, where shock waves are prone to form, and flow complexity significantly increases. To fully evaluate the model's predictive adaptability and robustness across varying flow characteristics, these two conditions were selected as experimental scenarios.

First, the feature mutation nodes are determined using the PELT change-point detection algorithm to adaptively divide the input wind tunnel test data into multiple intervals. The penalty parameter is one of the key hyperparameters used to control model complexity. If the penalty value is too small, the algorithm may misclassify noise as change points, leading to overfitting. Conversely, if the penalty value is too large, it may overlook genuine change points, resulting in underfitting. To address this, the modified Bayesian Information Criterion (BIC)[19] selects the optimal penalty coefficient within the interval [0.3, 1.5]. The BIC information criterion formula is as follows:

$$BIC = 2\cdot \ln\left(\frac{sse}{n}\right) + k\cdot \ln n + \frac{k(k+1)}{n-k-1} \tag{9}$$

where n is the total length of the input time series, sse is the sum of squared errors across all segments; k is the number of segments after breakpoint division. To satisfy the requirements of sufficient fit quality and model complexity control, the penalty coefficient yielding the minimum BIC value is selected for interval division. The optimal penalty coefficients obtained at Mach 0.3 and Mach 0.8 are 0.8053 and 1.3737, respectively.

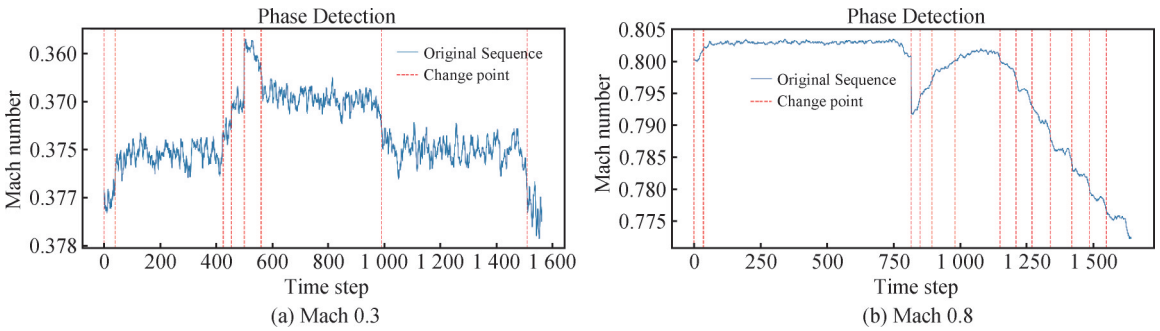

(a) Mach 0.3 (b) Mach 0.8

Fig.4 Interval division results of the PELT algorithm

Next, linear models were fitted to each interval, extracting the slope and residual standard deviation for each interval model. Based on these two interval characteristics, the K-means clustering method was applied

to group the intervals. A three-stage classification was then performed according to the characteristics of each cluster center. The feature patterns for each stage and the resulting sample sizes for each stage are shown below.

Table 1 Characteristics of Samples at Each Stage

Condition	Mach 0.3				Mach 0.8			
stage\indicator	Sample Size	Mean	Average Slope	Average Residual Standard Deviation	Sample Size	Mean	Average Slope	Average Residual Standard Deviation
start stage	60	0.3800	-0.000008	0.000100	35	0.7930	-0.000018	0.002013
steady stage	1445	0.3783	0.000003	0.000183	1110	0.8020	0.000026	0.000287
transition stage	53	0.3767	-0.000008	0.000293	496	0.7859	-0.000036	0.000415

To ensure the data length is consistent when plotting the 3D image, normalize the time of each interval to keep its time step length constant. The three-dimensional plots obtained from the experiments are shown in Fig.5.

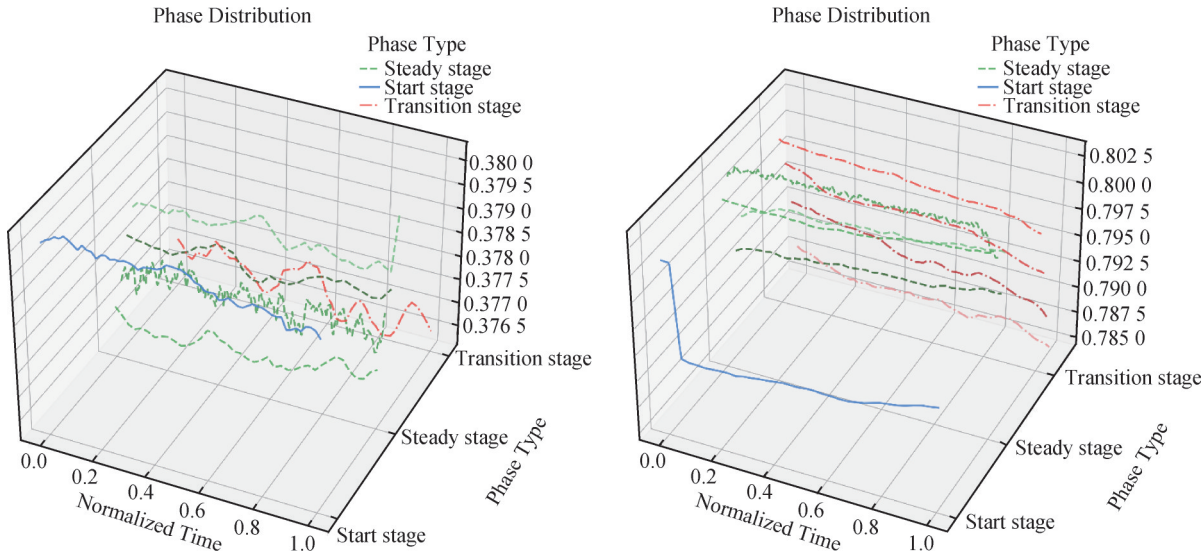

(a) Mach 0.3 (b) Mach 0.8

Fig.5 Three-dimensional display of data

For each phase, 70% of the overall data is selected as the training set and the remaining 30% as the test set to build the LSTM phase model and the unified global LSTM model, respectively. For this purpose, we need to perform data normalization first. The normalization method chosen in this paper is the departure normalization method, which applies a linear transformation to the original data so that the resultant values are mapped between [0,1].

$$x_{nor}=\frac{x_i-x_{min}}{x_{max}-x_{min}} \tag{10}$$

Where x_{max} denotes the maximum value in a set of sequences and x_{min} denotes the minimum value in a set of sequences. After the model output results, in order to compare the model output results with the actual output, the output results of the model are usually also subjected to the inverse normalization operation, and the formula for the inverse normalization is as follows.

$$x=x_{nor}(x_{max}-x_{min})+x_{min} \tag{11}$$

The LSTM network structure is optimized using the Adam optimizer. The Adam optimizer is an optimization algorithm with an adaptive learning rate. The core idea is to maintain two dynamic learning rates for different parameters, which are first-order moment estimation (i.e., mean) and second-order moment estimation (i. e., variance) based on the gradient. In this way, the Adam optimizer can adaptively adjust the learning rate for each parameter, making the training process more stable and efficient[20].

For each stage, a Mach number prediction model based on an LSTM network was constructed using five input variables—total pressure, static pressure, Mach number, angle of attack, and rotational speed—with Mach number as the output variable. The model comprises one input layer, one LSTM layer, one fully connected layer, and one regression layer.

The complete algorithm pseudocode is as follows:

Algorithm: PELT-Phase LSTM
Input: Multivariate time series D, window size N, Training epochs E = 500, Random seed = 42
Output: Phase-specific LSTM models

```
1 // Initialize with random seed
    Set random seeds(seed) for all frameworks
2 // Change Points Detection
    breakpoints = PELT_Detect(D, penalty_range)
    segments = Split_Sequence(D, breakpoints)
3 // Phase Clustering
    features = [slope, residual_std] for each segment
    phase_labels = KMeans(features, n_clusters=3, random_state=
seed)
4 // Phase-specific Training
    for each phase in [Startup, Stable, Transition]:
        X_phase, Y_phase = Extract_Phase_Data(phase)
// Adaptive configuration
        if |Y_phase| < 100:
            hidden_size = 64, lr = 0.008
        else:
            hidden_size = 200, lr = 0.003
        model = LSTM(hidden_size=hidden_size)
        for epoch = 1 to E:
            Train(model, X_phase, Y_phase, lr=lr)
    return phase_models
```

The RBF neural network is a single-layer feedforward network that employs radial basis functions as the hidden layer activation function. It locally partitions the input space through a set of learnable center parameters, with each center corresponding to a local region within the input space. The width parameter controls the influence range of this region. Input samples' distances from each center are transformed into local responses via radial basis functions, with stronger responses for closer distances. The final output is obtained by linearly weighting these local responses through the output layer.

MLP, or Multi-Layer Perceptron, is a classic fully-connected feedforward neural network comprising an input layer, multiple hidden layers, and an output layer. Neurons between layers are fully connected through learnable weights. The hidden layers employ the ReLU function for nonlinear transformation, endowing the network with universal approximation capabilities to fit complex nonlinear mapping relationships. As a static network, it requires flattening the input window into a one-dimensional feature vector when processing time series data.

This paper compares the phased model with global LSTM models, global RBF neural network models, and global MLP models. The comparison figures and experimental data for the prediction results of each phase are as follows.

The corresponding RMSE data results at Mach 0.3 are shown in Table 2.

The corresponding RMSE data results at Mach 0.8 are shown in Table 3.

As shown by the experimental results in Tables 3 and 4, the proposed PELT-Phase LSTM model significantly outperforms the global LSTM, global MLP, and global RBF models under both Mach 0.3 and Mach 0.8 scenarios, demonstrating higher accuracy in Mach number prediction tasks.

Under subsonic conditions at Mach 0.3, the PELT-Phase LSTM model achieved average RMSE reductions of 27.92%, 22.13%, and 60.17% compared to the other three models. This indicates that the model effectively captures the dynamic variation patterns of Mach number across different flight stages through phased modeling, thereby overcoming the shortcomings of global models in balancing commonalities and specific characteristics across stages. In transonic scenarios at Mach 0.8, the PELT-Phase LSTM model demonstrated even more pronounced advantages, achieving average RMSE reductions of 28.10%, 42.03%, and 83.43%. This outcome confirms the model's applicability not only to smoothly gradual dynamic characteristics in subsonic conditions but also to effectively handling strong nonlinear flow variations caused by phenomena like shock waves in the transonic region. By integrating the

Table 2 Comparison of Model RMSE at Mach 0.3

model	PELT-Phase LSTM	Global LSTM	Improvement Amount	Global MLP	Improvement Amount	Global RBF	Improvement Amount
start stage	0.0000582	0.0001882	**+69.0825%**	0.0000983	**+40.8073%**	0.0003861	**+84.9298%**
steady stage	0.0001046	0.0001072	**+2.4466%**	0.0001198	**+12.6712%**	0.0001501	**+30.2864%**
transition stage	0.0001043	0.0001189	**+12.2219%**	0.0001198	**+12.9264%**	0.0003006	**+65.2881%**

Table 3 Comparison of Model RMSE at Mach 0.8

model	PELT-Phase LSTM	Global LSTM	Improvement Amount	Global MLP	Improvement Amount	Global RBF	Improvement Amount
start stage	0.0000543	0.0001481	**+64.3394%**	0.0001943	**+72.0669%**	0.0002847	**+80.9323%**
steady stage	0.0001155	0.0001189	**+2.8296%**	0.0001614	**+28.4276%**	0.0006210	**+81.4034%**
transition stage	0.0001585	0.0001913	**+17.1310%**	0.0002130	**+25.5909%**	0.0013162	**+87.9580%**

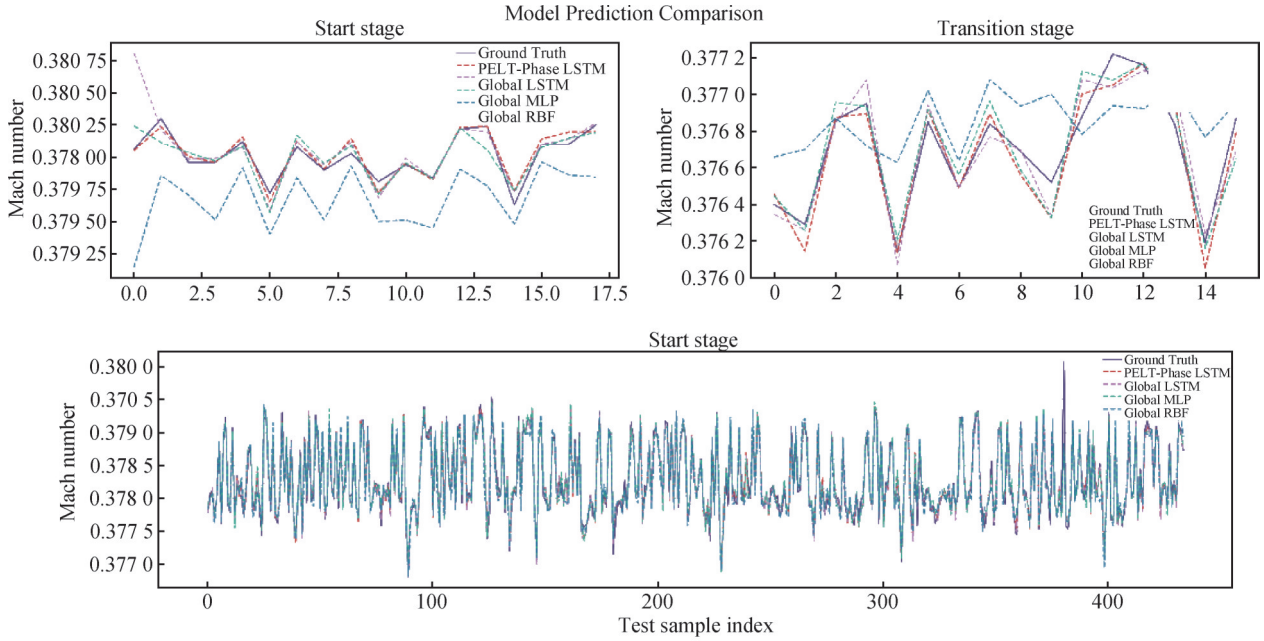

(a) Prediction comparison chart at Mach 0.3

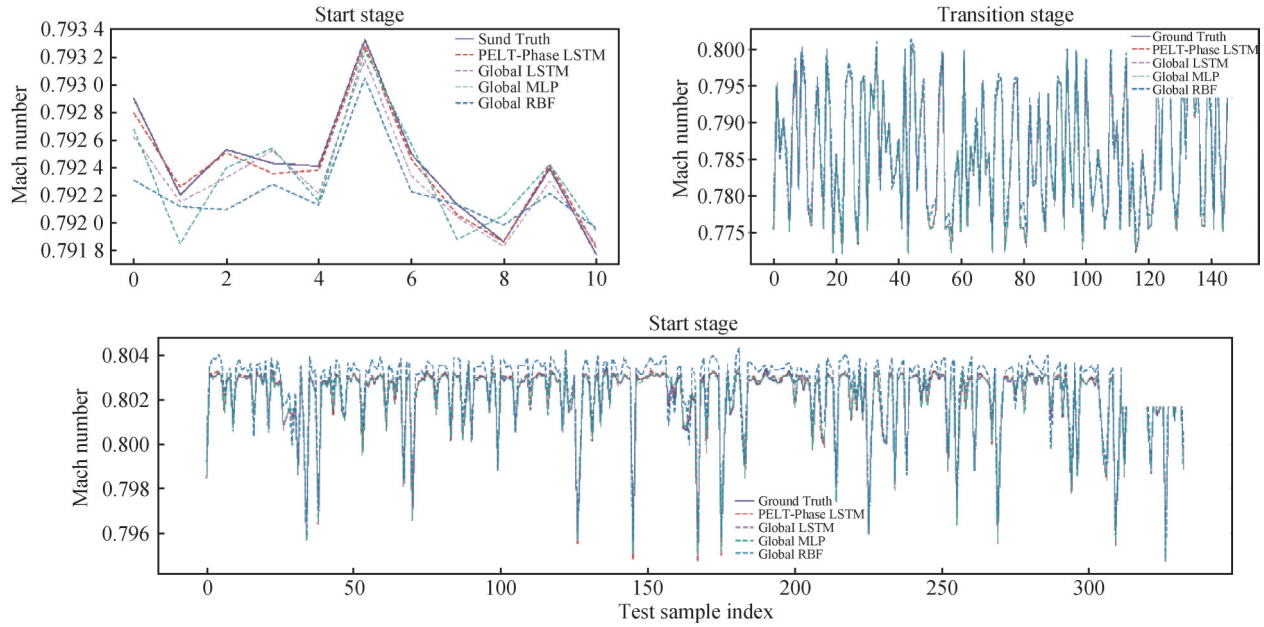

(b) Prediction comparison chart at Mach 0.8

Fig.6 Comparative experimental prediction diagram

PELT algorithm's variable-point detection capability with LSTM's advantage in modeling time-series features, the PELT-Phase LSTM model achieves high-precision prediction of dynamic behavior across all stages under varying Mach numbers. This fully validates the model's robust performance and generalization capability across operating conditions and multi-stage scenarios.

Given that phased modeling increases computational complexity and maintenance costs, it is necessary to compare and explain the computational time of different models.

It can be seen that in terms of computational efficiency, the stage-based LSTM requires training and maintaining three independent models, resulting in significantly higher computational time compared to other global models. However, this increased computational cost yields a substantial improvement in prediction accuracy. As demonstrated in the preceding experiments, the phased LSTM achieves substantially

Table 4 Comparison of Computation Times

Model\Scenario	Mach 0.3	Mach 0.8
PELT-Phase LSTM	3.562 s	3.555 s
Global LSTM	0.947 s	1.746 s
Global MLP	0.753 s	0.734 s
Global RBF	0.743 s	0.740 s

lower RMSE than the global model at both Mach 0.3 and Mach 0.8. This trade-off indicates that the phased LSTM is better suited for industrial scenarios demanding stringent prediction accuracy with relatively abundant computational resources. Conversely, when applications prioritize extreme real-time performance over high precision, the lightweight advantage of the global model becomes more pronounced.

5 Conclusion

Considering the three-dimensional characteristics of the continuous wind tunnel data and the significant phase characteristics presented by the Mach number, this paper proposes a model that integrates the PELT change-point detection algorithm with the phase LSTM network. The model first identifies the characteristic change points of the Mach number sequence through the PELT algorithm and divides them into intervals, then divides the data into three phases, namely, the start stage, the steady stage, and the transition stage, according to the characteristic law of each interval, and establishes the corresponding phase-specific LSTM modeling. Experimental results demonstrate that the proposed method achieves significantly lower RMSE across all stages compared to global LSTM, MLP, and RBF models under Mach numbers of 0.3 and 0.8, exhibiting outstanding predictive performance.

Author Contribution:

Zhao Luping: Conceptualization, Data curation, Funding acquisition, Investigation, Methodology, Project administration, Supervision. Li Tingting: Methodology, Resources, Software, Validation, Formal analysis, Visualization, Writing-original draft, Writing-review & editing.

Acknowledgments:

All data were provided by the Aviation Technology Key Laboratory of Aerodynamics Research in High-Speed and High Reynolds, Shenyang 110819, China.

Foundation Information:

This research was funded by the National Natural Science Foundation of China (No. 61503069) and the Fundamental Research Funds for the Central Universities (N2404010).

Data Availability:

The data that support the findings of this study were provided by a third party under a confidentiality agreement and therefore cannot be made publicly available. Data access may be requested from the corresponding author, subject to permission from the data provider.

Conflicts of Interest:

The authors declare no competing interests.

Dates:

Received July 13, 2025; Accepted March 30, 2026; Published online July 10,2026.

References

[1] Wang X. J., Yuan P., Mao Z. Z., & Du N. (**2016**). Wind tunnel Mach number prediction model based on random forest [J]. *Journal of Aeronautics*, 37(5), 1494-1505.

[2] Ren X., Hu P., Su H., Zhang F. Z., & Yu H. H. (**2024**). Physics-informed neural networks for transonic flow around a cylinder with high Reynolds number [J]. *Physics of Fluids* , 36 (3), 036129.

[3] Zhao L., Shao Y., & Jia W. (**2023**). NARX-Elman based Mach number prediction and model migration of wind tunnel conditions [J]. *Aerospace* , 10(6), 498.

[4] Gao H., Liu X. J., Guo J., & Lyu H. Q. (**2019**). Mach number control of continuous wind tunnel based on Gaussian process regression [J]. *Acta Aerodynamica Sinica*, 37(3), 480-487.

[5] Wang X. J. Two-Stage Time Series Mach Number Prediction Method Based on Recursive Pseudo-NARX and NARX. *No* .112378618B, China, **19** July 2022.

[6] Ju X. F., Wang X. L., & Gao Y. (**2018**). Multi-model-based predictive control method for wind tunnel flow field modeling [J]. *Control Engineering*, 25(10), 1830-1835.

[7] Sun S. J., Li X. L., Liu Y. M., Wang J. H., & Wang S. T. (**2023**). Influence of wide-speed-range inflow on aerodynamic performance of supersonic through-flow fan cascade [J]. *Acta Aeronautica et Astronautica Sinica*, 44(21), 528523-528523.

[8] Hang T. X., Ma Y. W., Chen H. X., Wang K. X., Pan Z. Y., & Hou D. W. Method and device for predicting Mach number of wind tunnel based on convolutional neural network. *No* .112560355, China, 11 May 2021.

[9] Du N., Yu W. S., & Yang X. R. (**2017**). Application of NARMAX model in the process of wind tunnel flow field modeling [J]. *Military Automation*, 36(11), 52-55.

[10] Rui W., Du N., Yuan P., Yi F., & Jin Z. W. (**2015**). Modeling and simulation of flow field control system in a transient-flush high-speed wind tunnel[J]. *Experimental Fluid Mechanics*, 6, 89-95.

[11] Wang T. J., Shi Y. D., Deng Z. Q., & Huang B. X. (**2016**). Preliminary study on energy-saving layout for conventional hypersonic wind tunnel [J]. *Journal of Experiments in Fluid Mechanics*, 30(6), 71-75, 104.

[12] Xie Z. F., Wei H., Zhu H. T., Yang F., Wu S. F., Zhou L. Y., & Li C. (**2025**). High-speed railroad curve control point identification method based on PELT and robust estimation [J]. *Railway Standard Design*, 1-9.

[13] Li X. W., Hou S. Z., Niu W. D., & Cui N. (**2025**). A combined PELT-GM-SARIMA highway freight turnover prediction model incorporating mutation point correction [J]. *Shandong Science*, 1-11.

[14] Chen W. Y., & Hu Y. (**2022**). Research on traffic flow state

detection and short-term prediction based on PELT [J]. *Highway Transportation Science and Technology*, 39(01), 120-129.

[15] Hochreiter S., & Schmidhuber J. (**1997**). Long short-term memory [J]. *Neural Computation*, 9(8), 1735-1780.

[16] Du X. Q., Lu Y., Dong H. T., & Hu C. Y. (**2025**). Prediction of wind pressure time series on square cylinder upon long short-term memory neural network [J]. *Engineering Mechanics*, 42 (4), 130-138, 186.

[17] Zhang J. J., Huang J., Liu Z. Q., Wang Q. F., & Chen B. (**2025**). A migration learning-based approach for variable confidence aerodynamic modeling[J]. *Experimental Fluid Mechanics*, 1-12.

[18] Lei P. F., Chen J. M., Hu Y. H., & Zhou E. (**2024**). Aerodynamic performance analysis of continuous wind tunnel with combined operation of main and auxiliary compressors [J]. *Journal of Aerospace Dynamics*, 39(12), 27-34.

[19] Zhang N. R., & Siegmund D. (**2007**). A Modified Bayes Information Criterion with Applications to the Analysis of Comparative Genomic Hybridization Data [J]. *Biometrics*, 63 (1):22-32.

[20] Li M., Lai G. H., Chang Y. M., & Feng Z. Q. (**2022**). Performance analysis of different optimizers in deep learning algorithms [J]. *Information Technology and Informatization*, (03), 206-209.